Materials Corrosion and Mitigation Strategies for APT:

Corrosion of Tungsten in an 800 MeV Proton Beam at the Weapons Neutron Research Facility

R. Scott Lillard, Darryl P. Butt
Materials Corrosion & Environmental Effects Lab
MST-6, Metallurgy

Gordon Willcutt
TSA-10

Phil Ferguson
LER-MLNSC

Luke Daemen
LANSCE-LER

Gary Kanner
MST-6

Los Alamos National Laboratory
Los Alamos, New Mexico 87545

submitted to:

Paul Lisowski
APT Project Office

March 14, 1996

Executive Summary

Real time electrochemical impedance spectroscopy data were acquired for a tungsten target during proton irradiation in the Weapons Neutron Research Facility at LANSCE. These impedance spectra were generated prior to irradiation and during irradiation beam currents of 50, 151, 350, and 484 nA. The data show that both the oxide impedance and charge transfer resistance (inversely proportional to metal dissolution rate) decrease with increasing beam current. These observations are consistent with three possible proton beam effects: 1) an increase in surface temperature of the tungsten target, 2) photoelectric effects and, 3) radiation induced conductivity of the native oxide which forms on W. Energy deposition and thermal hydraulic calculations predict that the surface temperature of the tungsten target was less than 31°C at the maximum beam current. This temperature is too low to fully account for observed changes. Moreover, substantial changes were observed at beam currents as low as 50 and 151 nA. The observed decrease in oxide resistance and increase in metal dissolution rate (with increasing beam current) is also consistent with radiation induced conductivity. Photoelectric effects, which may have arisen from fluorescence of the cell or solution, are usually associated with increased resistance to corrosion. Here, a decrease in corrosion resistance with increasing beam current was observed.

Because the amount of beam time originally allocated for these experiments was limited, the results presented here are preliminary. More extensive research in this area is planned for early June of 1997.

Introduction

Radiation Damage in Materials It has been demonstrated, for heavier and more energetic particle irradiation (i.e. for protons, neutrons, electrons, and ions), that radiation damage in materials generally takes one of 2 forms: 1) binary elastic / inelastic collisions and 2) electronic excitations. Several excellent reviews of this topic may be found in the literature**[1**,**2**,**3]**. Binary elastic collisions occur at lower particle energies and result in damage such as embrittlement, swelling, and amorphitization in both metals and other materials. Electronic excitations occur at higher particle energies and result in light transmission, dielectric loss, changes in dielectric constant, and both permanent and transient increases in electrical conductivity.

Radiation induced conductivity (RIC) changes occur when the valence electrons of an insulating or semiconducting material are promoted into the conduction band. For metals, the geminate recombination**[4]** of electron-hole pairs is to sufficiently fast (femptoseconds) such that electronic excitations are not an issue. In insulators and semiconductors, a sufficient number of the excited electrons and their associated holes recombine somewhat slower, on the order of pico-seconds, such that they available to migrate in an electric field. The lifetime of these charge carriers is still relatively short, most are less than 10^{-9}s and thereby limiting the enhanced conductivity to the time of irradiation though in some materials they may have lifetimes of several days.

Effect of Proton Irradiation on Electrode Potential M.Simnad and R. Smoluchowski investigated the effects of a 260 MeV proton beam on the open circuit potential of a tungsten target**[5]**. The sample was 0.012" in diameter, annealed at 900^{o} C and degreased before being placed in the cell. Electrode potentials were measured with respect to a saturated calomel cell by means of a vacuum tube potentiometer. The electrolyte was an oxygen-free, saturated KCl solution. They found for 260 MeV protons at increasing proton fluences that the potential of the tungsten sample became more positive (anodic) as shown in Table 1.

Table 1 Effect of 260 MeV protons on the open circuit potential of tungsten (from ref. **[5]**).

Sample Number	**Proton Fluence (p/cm^2)**	**Change in W Potential (mV)**
0	0	0
1	$1.8x10^{15}$	39
2	$6.8x10^{15}$	47
3	$2.2x10^{16}$	84

Their interpretation of the data was that the radiation field creates defects at the metal surface which contribute, somehow, to the electrode potential increase. They theorize that the defects have to be large (dislocation lines or loops, or collapsed vacancy clusters) because isolated vacancies and interstitial would presumably disappear rapidly given their proximity to the surface. In order to test the hypothesis that defects at the metal surface are responsible for the change in potential, they took a fourth sample, irradiated it, then, after the irradiation, annealed it at 900° C. After the annealing period the measure the electrode potential of the W sample and found that it returned to its original value. They concluded that the damage (and the corresponding enhanced corrosion) is reversible and can be "baked out".

A similar study on the proton irradiation of iron,**[6]** addressed metal dissolution rates. The electrolyte was a pH 2, HCl solution. A fluence of $1x10^{16}$ p/cm^2 leads it was found that the dissolution of the Fe_2O_3 layer at the surface of an iron electrode, an increase from 0.4 mg/cm^2 to about 1.4 mg/cm^2.

Focus of this Investigation In this investigation Electrochemical Impedance Spectroscopy (EIS) was used to characterize changes in the charge transfer resistance and the oxide film for a tungsten sample as a function of beam current at the LANSCE Weapons Neutron Research facility (commonly referred to as the Blue Room). These experiments are complimentary to those which

will be performed during the LANSCE A6 Target Station irradiation experiments scheduled to begin in March, 1997.

Electrochemical Impedance Spectroscopy is a powerful non-destructive technique for measuring the corrosion rates of metals in aqueous environments**[7**,**8**,**9]** and is ideally suited for systems with high solution resistivity. In EIS a small sinusoidal voltage perturbation (10 - 30 mV) is applied across the sample interface as a function of frequency. By measuring the transfer function of the applied ac voltage perturbation and the ac current response of the material, an impedance results ($Z\omega=V\omega/I\omega$). In the simplest sense, at low frequencies the material behaves as a resistor and $Z\omega=(R_{sol}+R_{pol})$ where R_{sol} is the ohmic resistance due to the solution and R_{pol} is the charge transfer resistance due to metal dissolution. At high frequencies, the material behaves as a capacitor and, therefore, offers no resistance to current. As a result $Z\omega=R_{sol}$. By measuring $Z\omega$ over a wide frequency range the solution resistance can be subtracted from the polarization resistance. From R_{pol} the corrosion rate (CR) for a sample can be determined from the relationship: $CR=A(1/R_{pol})$ where **A** is a constant.

This description of EIS assumes that the system being investigated behaves as a simple Randle's circuit. This circuit may be characterized by its electrical equivalents: a series resistor representing the geometric solution resistance which acts in series with a parallel resistance and capacitance representing the charge transfer and double layer capacitance. Most electrochemical systems, however, do not behave in this manner. This is not, however, a drawback rather an advantage of EIS. Specifically, it allows the investigator to characterize many of the properties of an electrochemical system in addition to the charge transfer resistance and the double layer capacitance. Specifically, changes in the passive film.

Experimental

Experiments were conducted in the Weapons Neutron Research facility at LANSCE. This facility provided easy access to a proton beam for a conventional three electrode electrochemical cell (discussed below). The proton beam measured approximately 1-2 cm in diameter (σ=4-8 mm) and had an energy of 800 MeV. The proton beam had a characteristic macropulse repetition rate of 20 Hz and a gate length of 625 microseconds (Figure 1). Beam currents were controlled by varying the spacing between each micropulse (and therefore the number of micropulses) in the gate. Nominally, the currents varied between 50 and 500 nA (Figure 1).

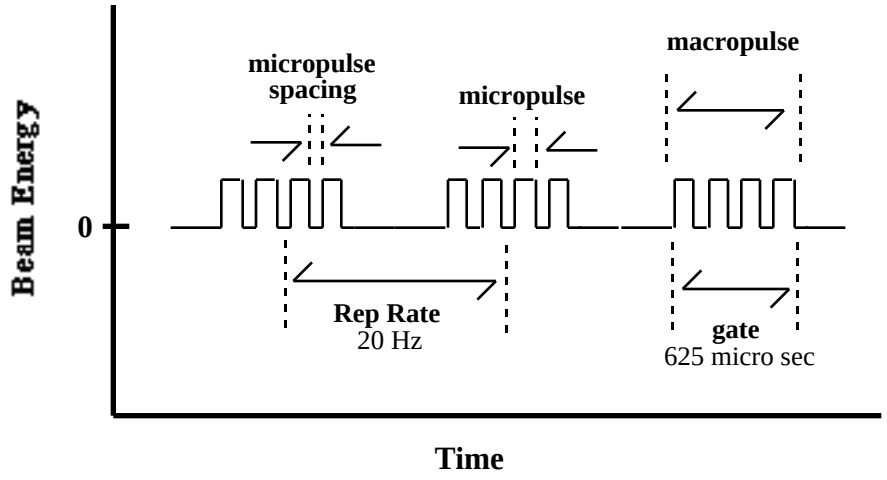

Micropulse Spacing (micro sec.): 50 nA - 10
141 nA - 3.6
351 nA - 1.4
484 nA - 1.1

Figure 1 Diagram depicting proton beam profile at the Weapons Neutron Research facility at LANSCE. The spacing between each micropulse is also given with respect to the proton beam current in nA.

A "half-round" tungsten sample was fabricated from a 99.96% tungsten rod 1/8"in diameter (Figure 2a). This sample served as both the proton beam target and the working electrode (WE) for our electrochemical measurements. The flattened region of the half-round sample faced the beam and measured 2 cm x 0.31 cm. The total surface area exposed to solution measured 1.7 cm^2. No masking of the sample was employed to minimize solution contamination

(from radiation damage) or crevicing. The sample volume exposed to the proton beam was approximately equal to 0.614 cm^3. The three electrode electrochemical cell used in these experiments is shown in Figure 2b. In addition to the W target, this cell also contained a platinum mesh counter electrode (CE) and a Saturated Calomel (SCE) reference electrode (RE). It has been reported that SCE maintains its stability after gamma irradiation at integrated dose rates of $1x10^4$ to $9x10^8$ rads**[10]**. Here, some discoloration of the plastic parts in the SCE (Vicor tip, shrink tubing, SCE body) was noted after the irradiation period but no structural damage to them or the cotton wadding was observed. The

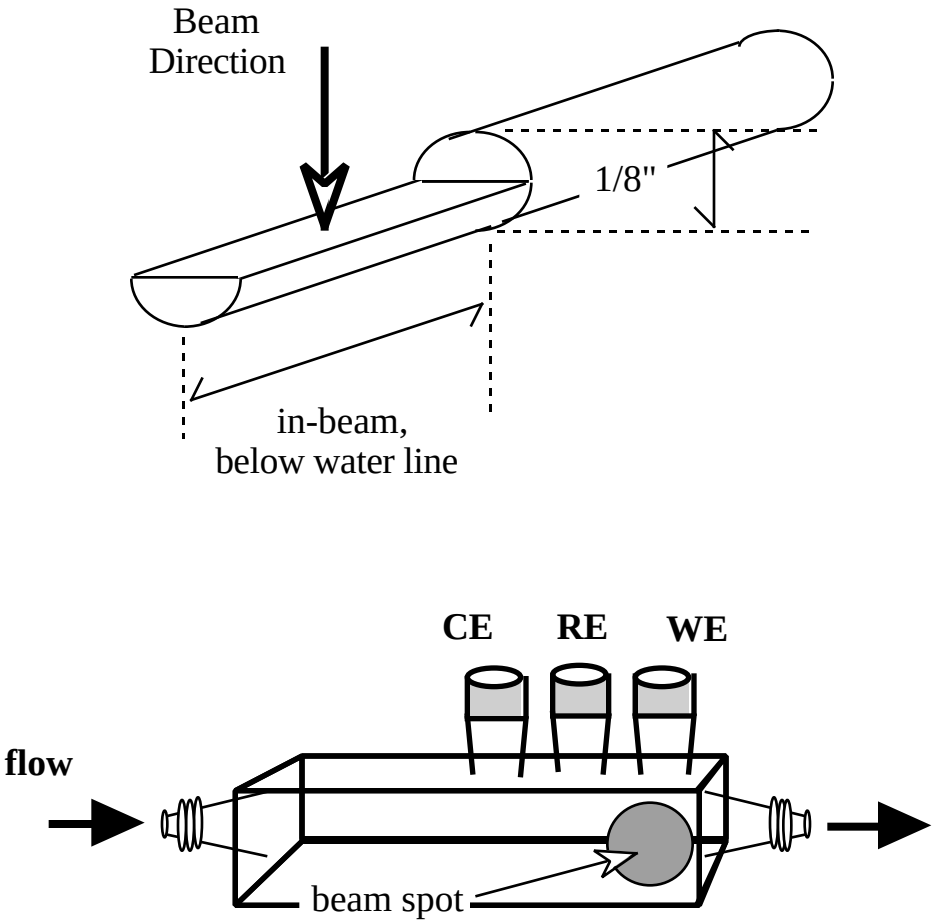

Figure 2 Diagrams depicting **a)** "half-round" tungsten target and **b)** electrochemical flow cell used in WNR irradiation experiments. WE denotes working electrode (W target), RE denotes reference electrode (SCE) and, CE denotes counter electrode (platinum mesh).

solution (0.1M NaCl) was pumped through the cell (and across the W target) at a rate of 1.02 L/min with a peristaltic pump. This was done to minimize build up of radiolysis products and heating of the W target due to energy deposition from the proton beam. The maximum cell temperature recorded during the irradiation was 26.0° C. Room temperature was approximately 24.5° C.

All electrochemical measurements were performed with a floating ground system. This was done to eliminate errors that may have been cause by ground loops.

Results and Discussion

Effect of Beam current on the Open Circuit Potential The open circuit potential (OCP) for tungsten in the WNR flow cell as a function of time is shown in Figure 3. When the proton beam was turned on (2 nA beam current) to align the cell with the beam center line a small positive shift in the OCP from its steady state value of -0.305V SCE to a value of -0.295V SCE was observed. After alignment, the OCP began to decrease towards its original value. As shown in Figure 3, soon after alignment the proton beam was turned on at 50 nA. Correspondingly, a large positive increase in the OCP was observed. While the OCP for W shifted to more positive potentials with increasing beam current, the absolute change decreased and appeared to plateau around -0.220V SCE (Figure 4). However, because the sample was polarized to 0.0V SCE between OCP measurements the accuracy of the measurement above 50 nA is uncertain.

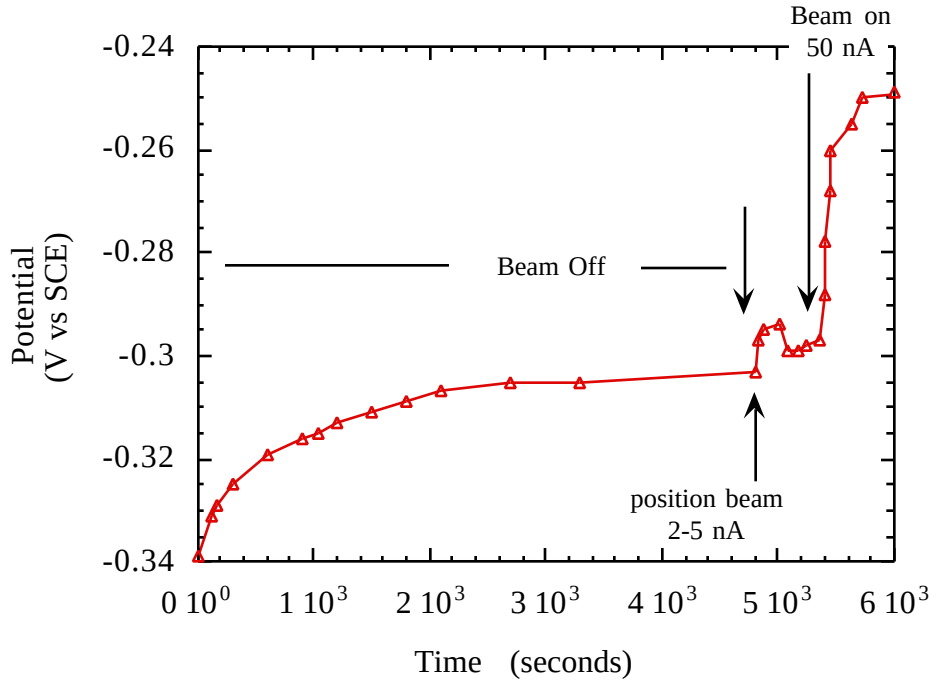

Figure 3 Open circuit potential for W in flow cell with 0.1M NaCl. Plot shows pre-beam values, change in OCP during positioning of beam and, value during irradiation at 50 nA.

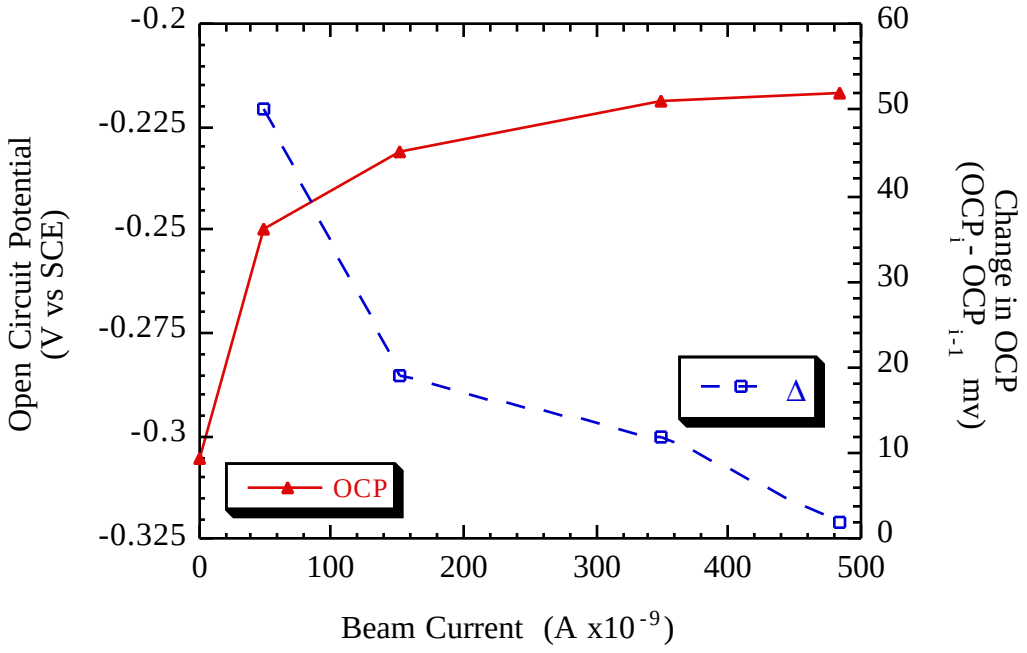

Figure 4 Open circuit potential for W in 0.10M NaCl as a function of proton beam current. Plot also shows change in open circuit potential from previous value as a function of beam current.

Proton Beam / Tungsten Oxide Interactions Because EIS measurements at the OCP ***may not*** have distinguished between increases cathodic reaction kinetics (which will result from hydrogen peroxide production) and radiation "enhanced" anodic reaction kinetics, all EIS experiments for W reported in this paper were measured at an applied anodic potential of 0.0 V SCE. This potential is near the anodically limited dissolution rate for W in 0.10M NaCl (Figure 5).

Typical EIS data before the beam was turned on and for beam currents of 141nA and 484nA are presented in Figure 8 in the form of Nyquist plots. These graphs plot the imaginary impedance as a function of the real component of the impedance. Recall that impedance, Z(ω), has both real and imaginary components:

$$Z(w) = Z_{real} + jZ_{imag}$$

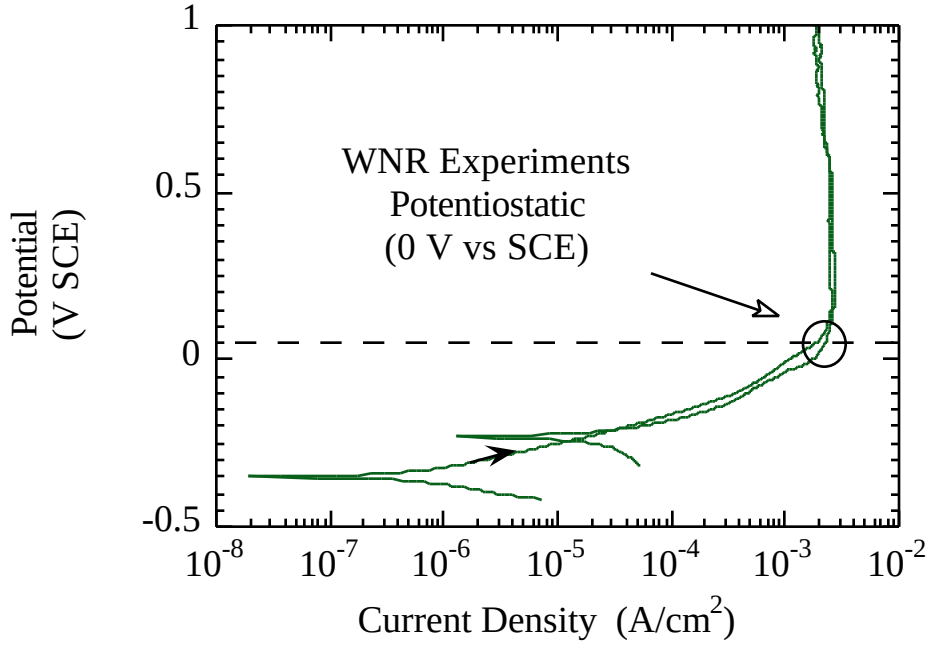

Figure 5 Potentiodynamic polarization curve for tungsten in 0.10M NaCl. Forward and reverse scan directions are indicated by arrows.

where Z_{real} and Z_{imag} are the real and imaginary components respectively and $j = (-1)^{1/2}$. In Figure 6 Z_{real} is symbolized by Z' and the Z_{imag} by Z". As seen in Figure 6, there is a precipitous decrease in impedance of the tungsten target at any one frequency as beam current is increased.

For any one plot in Figure 6, each semicircle may be characterized by its electrical equivalent, a resistor and capacitor in parallel. Therefore, the tungsten system may be represented by the electrical equivalent circuit present in Figure 7. In this figure the charge transfer resistance, R_{ct}, and the double layer capacitance, C_{dl}, represent the electrochemical reactions at the solution / oxide interface and R_{ox} and C_{ox} represent the intrinsic properties of the native oxide film which naturally forms on W.

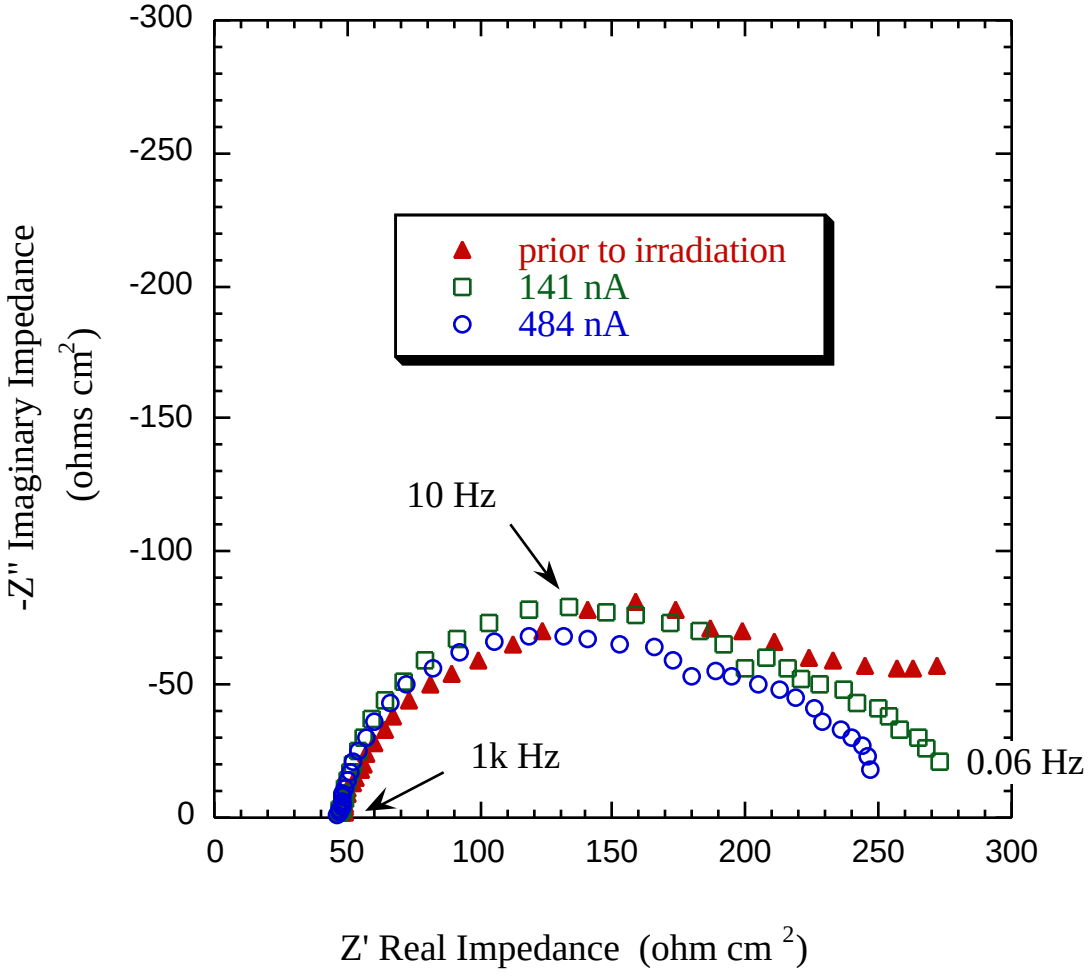

Figure 6 Nyquist plots for the WNR tungsten target in 0.10M NaCl as a function of proton beam current.

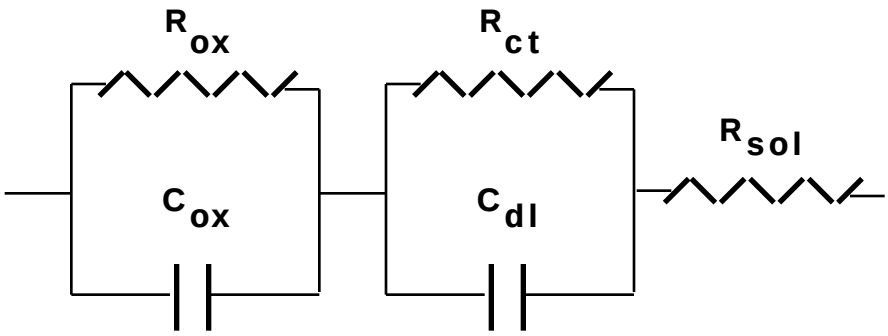

Figure 7 Electrical equivalent circuit representing the tungsten corrosion system where: R_{ox} represents the resistance of the oxide, C_{ox} represents the capacitance of the oxide, R_{ct} represents the charge transfer resistance (inversely proportional to metal dissolution rate), and C_{dl} represents the double layer capacitance. R_{sol} represents the geometric solution resistance.

A typical curve fit for the tungsten data at a beam current of 350 nA to this model is presented in Figure 8. The high frequency time constant (semi-circle) reflects the impedance response of the tungsten oxide while the low frequency semi-circle is due to metal dissolution (i.e. the charge transfer resistance and double layer capacitance). As shown in Table 2, both the oxide resistance and charge transfer resistance decrease with increasing beam current. Currently we are pursuing three separate explanations for this observed decrease in oxide resistance and increase in metal dissolution rate with increasing beam current:

1) Energy deposition (temperature effects)
2) Fluorescence of cell / solution (photoelectrochemical)
3) Radiation induced conductivity in the passive oxide

In the following sections each of these mechanisms is discussed in some detail. Furthermore, each of these issues will be addressed experimentally in our June ‘97 WNR beam time.

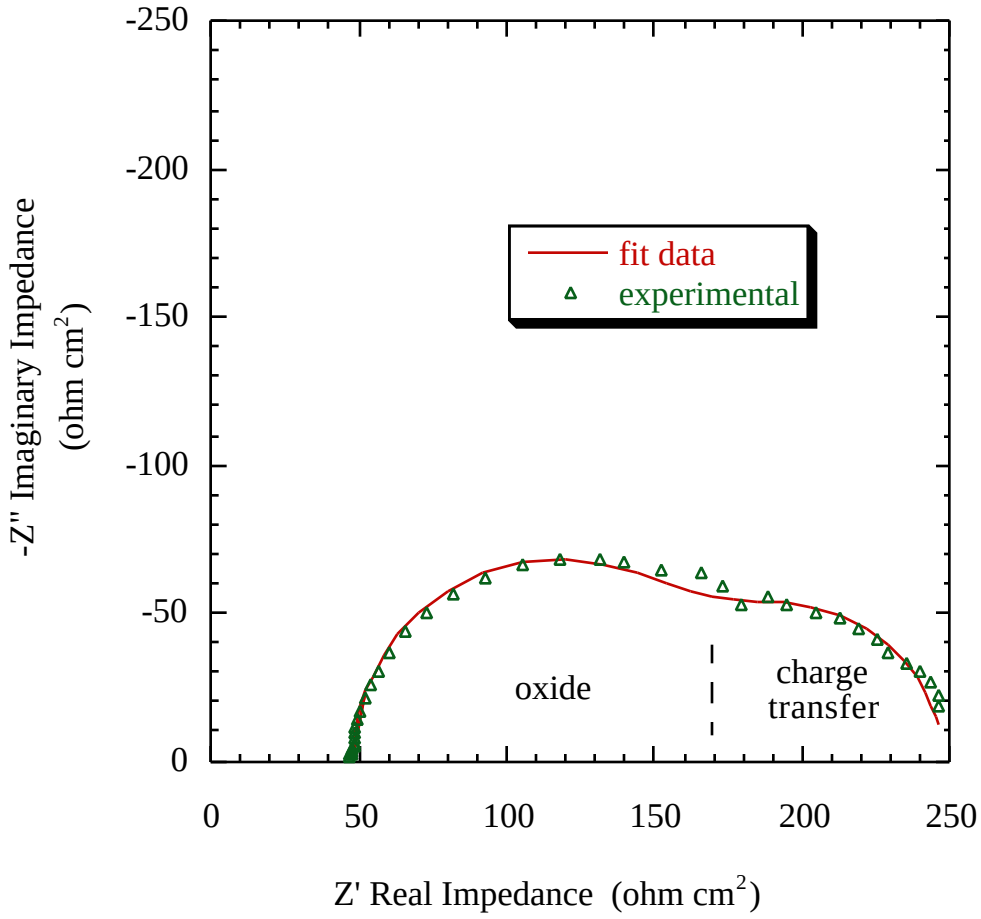

..

Figure 8 Nyquist showing the tungsten target in 0.10M NaCl during irradiation at 484 nA and the fitted data based on the EC presented in Figure 7. As shown in this figure, the high frequency time constant was attributed to the oxide while the low frequency time constant was attributed to the charge transfer resistance.

Table 2 Curve fit data for the WNR tungsten target in 0.10M NaCl as a function of beam current.

Beam Current nA	**R_{ox} ohm cm^2**	**R_{ct} ohm cm^2**
pre-irradiation	174	diffusion
50	146	89
151	139	84
350	123	82
484	119	80
1 hr post	140	88
12 hr post	178	95

Energy Deposition and Thermal Hydraulic Calculations To determine the effects of energy deposition (from the proton beam) on the surface temperature of the tungsten target, energy deposition and thermal hydraulic calculations were performed. The distribution of beam energy across the sample is Gaussian in nature. Assuming a sigma of 4mm (2σ=0.8cm) the peak power density at a beam current of 1nA was calculated to be 3.36×10^4 W/m^3. This assumption is conservative, as the beam spot was likely closer to 2 cm in diameter as opposed to 1 cm. For the beam currents examined here the peak power densities were therefore: 1.68×10^6 W/m^3, 4.74×10^6 W/m^3, 1.18×10^7 W/m^3 and 1.63×10^7 W/m^3.

The solution velocity past the half round tungsten rod of diameter 0.318 cm for a cell ID of 1.9 cm x 1.9 cm and a solution flow rate of 17.07 cm^3/s (1.024 L/min) was 5.16 cm/s. For the remainder of the cell the velocity was approximately 4.73 cm/s. The Reynolds number for the minimum area around the W sample was 183 while that for the remainder of the cell was 168.

The heat transfer coefficients calculated for the given maximum and minimum velocities using a cylinder model**[11]** are 2667 and 2553 W/m^2-C respectively.

The estimated surface temperatures for the tungsten target were calculated using 2 approximations. The first assumes a half round rod of the diameter used in these experiments. The maximum surface temperatures (for a beam current of 484 nA) are 4.8° and 5.1° C above the water temperature (30.8° and 31.1° C). In this model the sample temperature distribution was determined to be essentially uniform as the ΔT from the center of the sample to the sample surface in this model was only 0.03° C. The second model used the actual half round rod geometry of the actual tungsten target and the assumption of uniform surface heat flux. For this model the maximum surface temperatures (for beam currents of 484 nA) were only 3.0 and 3.1° C above the water temperature (29.0° and 29.1° C). Because the reaction rate scales with RT/nF where T is the temperature in degrees Kelvin, from these results we can conclude that surface temperature effects are not a factor which must be considered in the in-beam experiments.

Fluorescence - Photoelectrochemistry During the course of our WNR experiments some luminescence of the target / cell was observed at higher beam currents. The source of this effect is unknown. It may have been due to interaction of the beam with quartz cell or possibly the interaction with the solution. For example, the proton beam may excite electrons in the quartz cell which, during their relaxation process, emit photons of various wavelengths in the UV-vis range (fluorescence). The passive oxide which forms on tungsten (WO_3) is a semiconductor with a band gap of 2.6 ev**[12]**, and has been shown to produce photoelectric currents when exposed to light from a Xenon lamp**[13]**. Photoelectrochemical effects are usually associated with increased resistance to corrosion. Here, a decrease in corrosion resistance with increasing beam current was observed.

Radiation Induced Conductivity Radiation induced conductivity measurements have found that the electrical conductivity of Al_2O_3 can be increased from its bulk value of 10^{-14} S/m to 10^{-6} S/m in

a proton beam at dose rates of 10^4 Gray/sec (absorbed dose/sec)**[14,15,16]**. This effect may be increased and even prolonged after the irradiation period if an electric field is applied across the ceramic / insulator during irradiation as shown by Pells et al**[17]** for $MgAl_2O_4$ spinel irradiated by an 18 MeV proton beam.

The observed decrease in R_{ox} with increasing beam current is consistent with RIC. The gradual increase in oxide resistivity after the beam was turned off would indicated that the RIC was transient, with a lifetime greater than 1 hour and less than 12 hours.

References

1 L.W. Hobs, F.W. Clinard, S.J. Zinkle, R.C. Ewing, **Journal of Nuclear Materials**, vol. 216, pp. 291-321, 1994.

2 D.R. Olander, Fundemental Aspects of Nuclear Fuel Elements, Technical Information Center, Office of Public Affairs, Energy Research & Developement Administration, 1976.

3 Hj. Matke, Science of Advanced LMFBR Fuels, North-Holland, Amsterdam, 1986.

4 V.A.J. van Lint, T.M. Flanagan, R.E. Leadon, J.A. Nabor, V.C. Rogers, Mechanisms of Radiation Effects in Electronic Materials, vol. 1, Wiley, New York, 1980.

5 M.Simnad and R. Smoluchowski, **Physics Review**, vol.99 pp. 1891-2, 1955.

6 M.Simnad and R. Smoluchowski, **Physics Review**, vol.98, pp.1961-2, 1955.

7 J.R. Macdonald, Impedance Spectroscopy, Wiley Publishing, New York, 1987.

8 I. Epelboin, C. Gabrielli, M. Keddam, H. Takenouti, "Alternating-Current Impedance Measurements and Corrosion Rate Determination", in Electrochemical Corrosion Testing, ASTM STP 727, F. Mansfeld & U. Bertocci eds., ASTM, Ohio, pg. 150-66, 1981

9 D.D. MacDonald, M.C.H. Mckubre, "Electrochemical Impedance Techniques in COrrosion Science" in Electrochemical Corrosion Testing, ASTM STP 727, F. Mansfeld & U. Bertocci eds., ASTM, Ohio, pg. 110-59, 1981

10 M.J. Danielson, **Corrosion**, vol. 51, no. 6, pp. 450-455, 1995.

11 Zhukasukas, A., "Heat Transfer from Tubes in Cross Flow," in J.P. Hartnettand T. F. Irvine, Jr., Eds., Advances in Heat Tranfer, Vol. 8, Academic Press, New York, 1972.

12 F.H. Jones, K. Rawlings, J.S. Foord, P.A. Cox, R.G. Egdell, J.B. Pethica, B.M.R. Wanklyn, **Physical Review B**, vol. 52, no. 20, pp. R14 392-395, 1995.

13 A. Goossens, D.D, Macdonald, **Electrochemica Acta**, vol. 38, no. 14, pp1965-68, 1993.

14 G.P. Pells, **Journal of Nuclear Materials**, vol. 184, pp. 177-182, 1991.

15 V.A.J. van Lint, J.W. Harrity, T.M. Flanagan, IEEE Transaction of Nuclear Science, NS-15, no. 6, pg 194, 1968.

16 T. Shikama, M.Nauri, Y. Edo, A. Ochiai, H. Kayano, **Journal of Nuclear Materials**, vol. 544, pp. 191-194, 1992.

17 G.P. Pells, **Journal of Nuclear Materials**, vol. 184, pp. 183-190, 1991.